Electronic defect study on low temperature processed $Cu(In,Ga)Se_2$ thin film solar cells and the influence of an Sb layer

L Van Puyvelde*[,a], J Lauwaert[a,b], A Tempez[c], W Devulder[a], S Nishiwaki[d], F Pianezzi[d], C Detavernier[a], A N Tiwari[d] and H Vrielinck[a]

[a] Department of Solid State Sciences, Ghent University, Krijgslaan 281, 9000 Ghent, Belgium

[b] Department of Industrial Technology and Construction, Faculty of Engineering & Architecture, Ghent University, Valentin Vaerwyckweg 1, 9000 Ghent, Belgium

[c] Horiba Jobin Yvon SAS, Avenue de la Vauve - Passage Jobin Yvon, CS 45002 - 91120 Palaiseau, France

[d] Laboratory for Thin Films and Photovoltaics, Empa, Swiss Federal Laboratories for Materials, Science and Technology, Ueberlandstrasse 129, CH-8600 Duebendorf, Switzerland

E-mail: Lisanne.VanPuyvelde@UGent.be

Abstract A way to lower the manufacturing cost of $Cu(In,Ga)Se_2$ (CIGS) thin-film solar cells is to use flexible polymer substrates instead of rigid glass. Because such substrates require lower temperature during absorber deposition, the grain growth of the absorber layer can be hindered which leads to a lower cell performance. Partial compensation of this efficiency loss might be accomplished by growing the absorber in the presence of Sb, which is reported to promote grain growth. In this work CIGS solar cells, deposited on glass substrates, at reduced substrate temperature with a thin Sb layer (7, 12 nm) on top of the Mo contact are investigated. The diffusion profile of Sb is measured with Plasma Profiling Time of Flight Mass Spectrometry. The beneficial effect of Sb on efficiency and grain size is shown in quantum efficiency measurements and with scanning electron microscopy, respectively. Electric spectroscopy is used to explore the possible effects on the defect structure, more in particular on the dominant shallow acceptor. Admittance spectra exhibit a capacitance step to the geometric capacitance plateau at low temperature (5-60 K). Analyzing this capacitance step, we obtained a good estimate of the activation energy of the intrinsic defects that provide the p-type conductivity of the CIGS absorber. The measurements did not show a change in the nature of the dominant acceptor upon Sb treatment.

Keywords: $Cu(ln,Ga)Se_2$, Defects, Admittance Spectroscopy, Sb layer

1 Introduction

Chalcopyrite $Cu(In,Ga)Se_2$ (CIGS) is among the most promising absorber materials for thin-film solar cells because of its direct and tunable energy band gap, high optical absorption coefficient in the visible to near-IR spectral range and high tolerance to defects and impurities. In order to reduce the large scale manufacturing costs and to enable affordable solar electricity, a roll-to-roll setup which produces flexible solar cells has great potential. Moreover flexible solar modules on polyimide have the potential to serve specialized consumer markets, like lightweight mobile device chargers (ideal for space applications) or for building-integrated photovoltaic systems. Record efficiencies of CIGS cells, both on glass (21.7% [1]) and on flexible substrates (20.4% [2]), already exceed 20%.

It was generally believed that high growth temperatures of about 600˚C are a prerequisite for reaching high efficiency CIGS devices. As the maximum applicable temperature for polyimide foils is restricted to below

500°C, different interdiffusion of elements and crystal growth takes place. Because of the resulting smaller grain sizes, more grain boundaries may act as recombination centres for photogenerated charge carriers, degrading the device performance. In this report an attempt was made to get high efficiency devices, despite low-temperature deposition processes, by adding an antimony layer on top of the Mo layer. Indeed, according to references [3-8] Sb can enhance grain size.

Besides the effect on grain size, it is reported in reference [9] that incorporation of Sb can alter the conductivity of CIGS. Because Sb doped $CuInS_2$ crystals are p-type, references [10, 11] suggest that the dominant shallow acceptor type defect can be assigned to a Sb atom on the S site (Sb_S).

So far optical characterization measurements on cells with an additional Sb layer underneath the CIGS absorber layer [12] could not reveal a direct effect of Sb on the defect structure. Therefore in this report, possible introduction of a shallow acceptor (Sb_{Se}), which could influence the electronic properties of CIGS, is investigated by low temperature admittance spectroscopy (AS).

In previous studies carrier freeze-out in CIGS layers was observed at low temperatures (< 50 K) and a shallow acceptor with an activation energy slightly below 30 meV was identified [13-15]. Based on density functional theory calculations Cu vacancies (V_{Cu}) were proposed to form this shallow acceptor [16]. The very efficient 'self-doping' ability of $CuInSe_2$ was attributed to the exceptionally low formation energy of Cu vacancies.

2 Experimental

CIGS thin-film solar cells were fabricated at Empa (Swiss Federal Laboratories for Materials Science and Technology). Sb was deposited by vacuum evaporation onto Mo coated soda lime glass. Sb precursor layers of 0, 7, or 12 nm thickness were synthesized, referred to as Sb0, Sb7 and Sb12, respectively. This Sb layer was coated with a thin Cu layer to prevent evaporation of Sb during early stages of the CIGS absorber deposition. The Na diffusion from the soda lime glass to the absorber might also be affected by the changed cell geometry. The experiments presented in this paper do not allow the effects of Na and Sb to be separated. These problems deserve further investigation. If experiments would be performed on PI foil, a distinct incorporation of Na (by NaF post deposition process) would be necessary. The CIGS absorber was grown by a low temperature multi-stage process. The average composition ratios for all three cells are around 0.86 for [Cu]/([Ga]+[In]) and 0.38 for [Ga]/([Ga]+[In]), as determined by X-ray fluorescence measurements. A substrate temperature of around 350°C was used during the first stage. The substrate temperature of the second and third stage was 450°C (normally around 600°C on glass). The CIGS absorber was covered with CdS by chemical bath deposition. The ZnO window layer and Ni/Al/Ni grid were deposited by RF sputtering and e-beam evaporation, respectively. No anti-reflection coating was applied.

For scanning electron microscopy measurements (SEM) a FEI Quanta 200F FEG-SEM was used. Depth profiling data were obtained with Plasma Profiling Time of Flight Mass Spectrometry (PP-TOFMS, Horiba Scientific). PP-TOFMS is, like SIMS (secondary ion mass spectrometry), a depth profiling technique based on material erosion and dynamic measurement of sputtered species. In PP-TOFMS a plasma source is coupled with a time of flight mass analyzer [17-19]. The intensity and energy of the commonly used Argon ions and fast neutrals causing material sputtering is much higher in PP-TOFMS compared to SIMS, leading to much faster analysis. Furthermore, in PP-TOFMS the sputtering and ionization processes in the discharge volume are two separate processes. As a result, PP-TOFMS is semi-quantitative for most inorganic materials. In SIMS only the ionized particles coming off from the material are collected and measured. As the distance between the Al/Ni grid and the Mo stripes is smaller than the size of the crater diameter (4 mm), samples were etched in 10% HCl prior to depth profiling in order to remove metal grid and front contact. External quantum efficiency measurements (EQE) were carried out under standard test conditions (1000W/m^2, 25°C) at room temperature in the 380-1180 nm wavelength range. Capacitance-frequency (C-f) measurements were performed with an Agilent impedance meter. Cells were measured in the relaxed state (in darkness for 1 h at room temperature) in the frequency range 100 Hz - 2 MHz and temperature range from 5 - 300 K. The capacitance was measured at dc biases of 0.6, 0.0, -0.3 and -0.6 V. A superimposed small ac voltage signal (30 mV) was used for probing the actual capacitance at the given bias.

3 Results and discussion

3.1 Solar cell characteristics

3.1.1 Solar cell parameters Device performance parameters (efficiency (η), open circuit voltage (V_{oc}), short circuit current density (J_{sc}), and fill factor (FF)) of the best cell on each sample are listed in the table 1. Series (R_s) and and shunt (R_p) resistance values are taken from measurements under illumination. An improvement in efficiency for cells with an additional Sb layer is obtained due to an increased J_{sc}, while V_{oc} is not altered much.

Table 1: PV parameters of the different solar cells.

sample	η(%)	V_{oc} (mV)	J_{sc} (mA/cm^2)	FF (%)	R_p (Ω/cm²)	R_s (Ω/cm²)
Sb0	12.1	641	28.8	65.7	704	0.8
Sb7	13.6	637	31.2	68.4	900	0.9
Sb12	13.5	646	31.8	65.9	712	0.9

3.1.2 Spectral response EQE measurements show an increase in carrier collection on the long wavelength side for cells with a Sb layer (Fig. 1). This provides an explanation for the increase in J_{sc} for these cells (table 1) and could be related to larger grain size (see further in Section 3.2.1). No obvious shift of the onset of

absorption is observed for cells with and without Sb layer. This is in accordance with reference [3]. References [6] and [9] on the other hand demonstrate a band gap decrease of $CuInS_2$ with increasing Sb doping. A linear extrapolation of squared EQE ($\alpha \propto (E-E_g)^2$) gives an estimate of the band gap at room temperature, which is around 1.14 $\pm$ 0.07 eV for all cells.

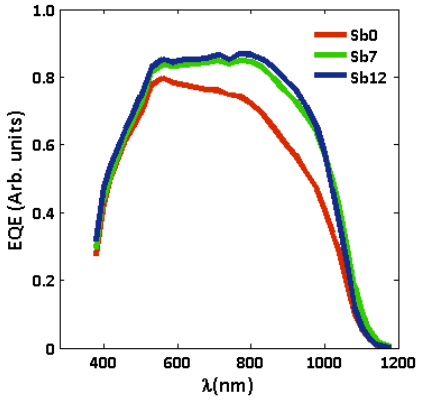

Figure 1: EQE of the investigated samples.

3.2 Absorber properties

3.2.1 Morphology SEM images (Fig. 2) show that grain size in samples with Sb layer is clearly larger than in the sample without Sb layer. Despite low substrate temperature during deposition, a large grain size can thus still be obtained by including Sb. Increased CIGS grain size with increasing Sb precursor layer thickness is in agreement with different reports [3-8]. The increased grain size and associated reduced grain boundary recombination might explain the improvement of the solar cell efficiency (due to larger J_{sc}) as shown in table 1. For all cells, the thickness of the absorber layers is around 2.1-2.2 µm.

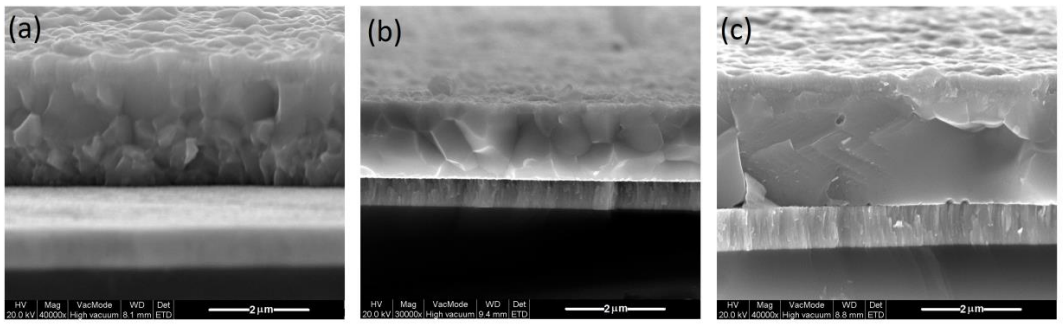

Figure 2: SEM micrographs of cross sections of the thin films
(a) Sb0, (b) Sb7 (after HCl etch) (c) Sb12.

3.2.2 Depth-dependent chemical composition Element depth profiles of Cu, In, Ga and Se of samples without (Sb0) and with (Sb12) Sb layer do not reveal large qualitative differences between these two cells. Nevertheless, for sample Sb12 the measurement reveals a clear diffusion profile of Sb, whereas for Sb0 the antimony signal remained below the detection limit. In order to illustrate this, the Ga and Sb profiles for the

two cells, applying the same scaling procedure, are shown in Fig. 3. From these measurements it becomes clear that indiffusion of Sb into the absorber layer is rather limited and most of the Sb remains in the layer on the Mo back contact. Nonetheless, a slight increase of the Sb concentration near the CIGS surface is also observed. Such concentration profile indicates that Sb has diffused through the CIGS absorber layer and hence may be compatible with the possibility of Sb enhancing the CIGS grain growth.

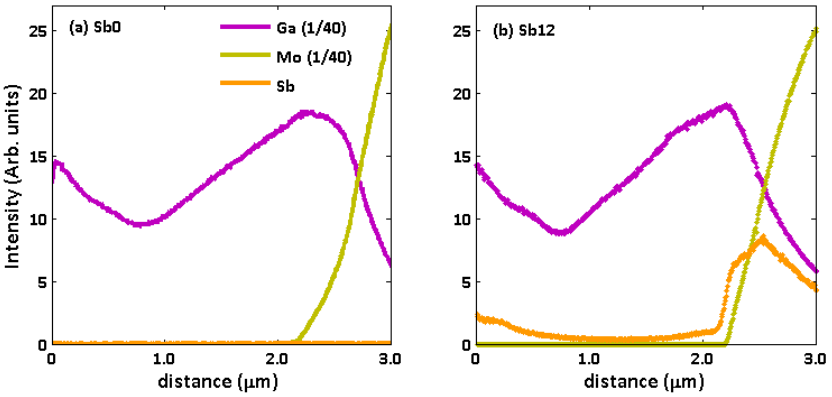

Figure 3: Ga, Mo and Sb depth profile signals of sample (a) Sb0, (b) Sb12.

3.3 Electronic defect characterization: Admittance spectroscopy

Admittance measurements performed in the temperature range from 5-250 K at a reverse bias of -0.3 V on Sb0 and Sb7 are presented in figures 4a and 5a, respectively.

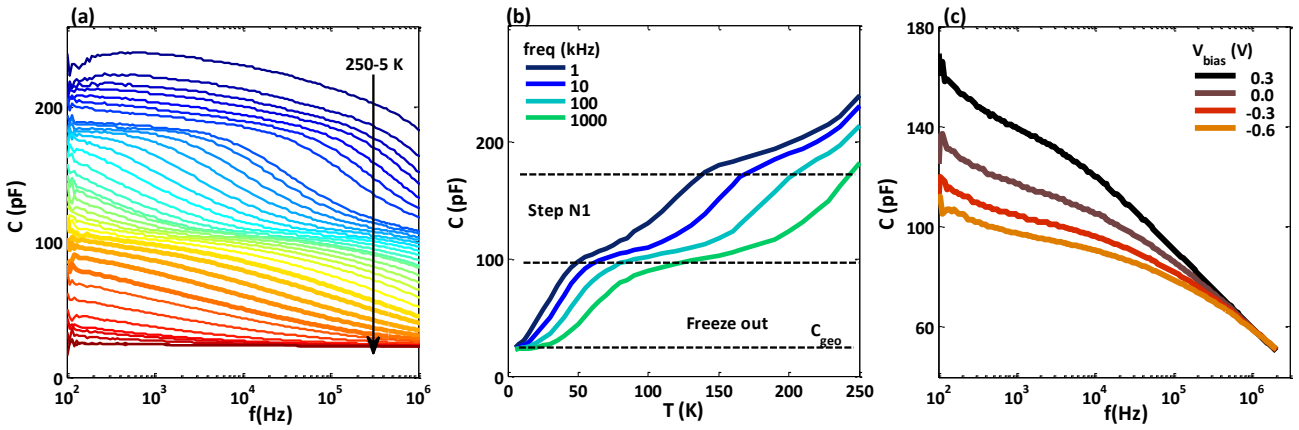

Figure 4: Admittance spectra and measured freeze-out for Sb0.

(a) C-f-T spectra for Vr =-0.3 V, (b) C-T for Vr =-0.3 V, (c) C-f at 60 K

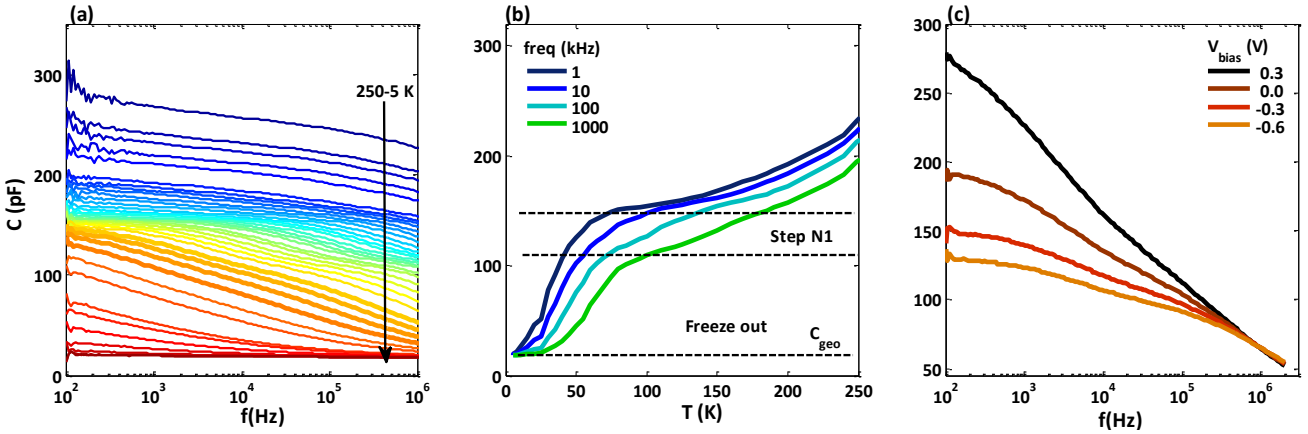

Figure 5: Admittance spectra and measured freeze-out for Sb7.
(a) C-f-T spectra for V_r =-0.3 V, (b) C-T for V_r =-0.3 V, (c) C-f at 60 K

In the C-f-T spectra for both samples, three capacitance steps can be discerned. Figures 4b and 5b, where capacitance is plotted as a function of temperature for different frequencies, show an onset of a third step at the highest temperatures (> 200 K), very probably related with very deep-level defects. At intermediate temperatures (120-165 K) a capacitance step occurs which is commonly observed in CIGS solar cells and labeled N1. Deep level transient spectroscopy measurements on these cells (not shown here) reveal an N1 signal that exhibits characteristics typical for a non-Ohmic contact, rather than for defects [20, 21]. We will not further discuss the assignment of this admittance step here, for which various interpretations have been suggested in literature [15, 22-25]. We will concentrate our attention on the step at lowest temperatures, here, though.

At the lowest temperatures (<100 K) and frequencies exceeding the dielectric carrier response frequency ($\omega_D = \sigma/(\varepsilon_0\varepsilon)$, σ being the conductivity, ε_r the relative permittivity and ε_0 the vacuum permittivity) the whole semiconductor behaves as a dielectric. The capacitance measured at such frequencies is the geometric capacitance $C_{geo} = \varepsilon_0\varepsilon_r A/d$, with d the thickness of the absorber and A the area of the cell [26, 27]. The step due to dielectric freeze-out is visible in C-f (figures 5a and 6a) and C-T spectra (figures 5b and 6b) for high frequencies (≈ 0.1-1 MHz) around 50 K. The dielectric freeze-out step can be distinguished from the other capacitance steps by its independence of applied bias on the high-frequency side of the step [26]. This independence is shown in figures 4c and 5c which present C-f spectra at 60 K for different bias.

For sample Sb0 and Sb7 a geometric capacitance C_{geo} of 2.25 10^{-11} F and 1.85 10^{-11} F, respectively, is reached (indicated in figures 4a and 5a) for a sample area of around 0.6 mm^2. If one calculates the thickness of the film (using ε_r = 10 [28]) values of 2.3 µm (Sb0) and 2.8 µm (Sb7) are derived, which are in quite good agreement with film thickness observed in SEM measurements (Fig. 2).

Using a circuit model [29] of a depletion region (W depletion region width) in series with the undepleted quasi-neutral region (thickness d-W) (additional series resistance is ignored), the characteristic frequency (ω_0) at which the capacitance exhibits a step due to dielectric relaxation of the absorber is calculated as

$$\omega_0 = \frac{W\,\sigma}{d\,\varepsilon}$$

As the conductivity can be expressed in terms of the product $qp\mu_h$, where q, p and μ_h are the elementary charge, the free hole density and mobility, respectively, the characteristic frequency, and hence freeze-out exhibits thermal activation due to combined contributions from mobility and carrier concentration. Following equation for the characteristic frequency is obtained [30].

$$\omega_0 = \frac{W\,q\mu_h\,N_v\,\exp\left(-E_a/kT\right)}{d\,\varepsilon}$$

$$\omega_0 = \xi_0\,T^m\,\exp\left(-E_a/kT\right) \qquad (1)$$

Here k is the Boltzmann constant, T is the absolute temperature, N_v the effective density of states in the valence band and E_a the energy distance between the shallow acceptor defect level (on which carrier freeze out occurs) and the valence band. From equation (1) it follows that the activation energy E_a of the intrinsic and perhaps extra Sb-doping-related shallow acceptor defects can be measured in the step at lowest temperatures which exceed 20 K (in order to have a large enough capacitance step above the geometric capacitance). E_a can be extracted from the plot of $\ln(\omega_0/T^m)$ versus 1/kT (Arrhenius diagram). The characteristic frequency is identified as the maximum of the differential capacitance $(-\omega/kT \cdot dC/d\omega)$ versus ω curve [27]. The differential capacitance curves corresponding to the C-f curves, indicated in bold in figures 4a and 5a, are shown in figure 6.

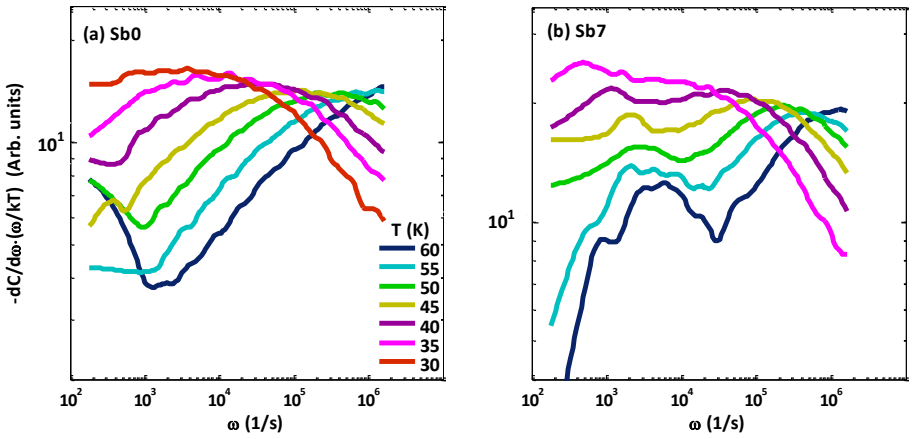

Figure 6: Differential capacitance calculated from C-f-T spectra for low temperatures (a) Sb0, (b) Sb7.

The exponent m for the Arrhenius diagram ($\ln(\omega_0/T^m)$ versus 1/kT) results from the temperature dependence of the effective density of states ($N_v \sim T^{3/2}$) and the temperature dependence of the mobility. If one assumes a temperature independent mobility (m = 3/2), the activation energies are 25 meV for Sb0 and 22 meV for Sb7 (figure 7a). An estimate of the error is made by comparing the values obtained taking m values between 0 and 3 (mobility determined by impurity scattering, $\mu_h \sim T^{3/2}$ [31]), we then estimate the error at 5 meV. The calculated activation energy is similar for both samples and around 25±5 meV. This value should yield a good

approximation of the activation energy of the shallow defect, responsible for the p-type conductivity of the CIGS layer. As, within experimental resolution, the activation energies derived from the low temperature capacitance step for the two samples are very similar, we conclude that Sb treatment did not change the activation energy of dominant acceptor defect. C-T data at a frequency of 100 kHz, normalized at T= 85 K after reduction of geometric capacitance (figure 7b), indeed show that the carrier relaxation for both samples is very similar. Following the interpretation of previous very similar experimental [13-15] and density functional modeling [16] results, we tentatively assign this level to the copper vacancy.

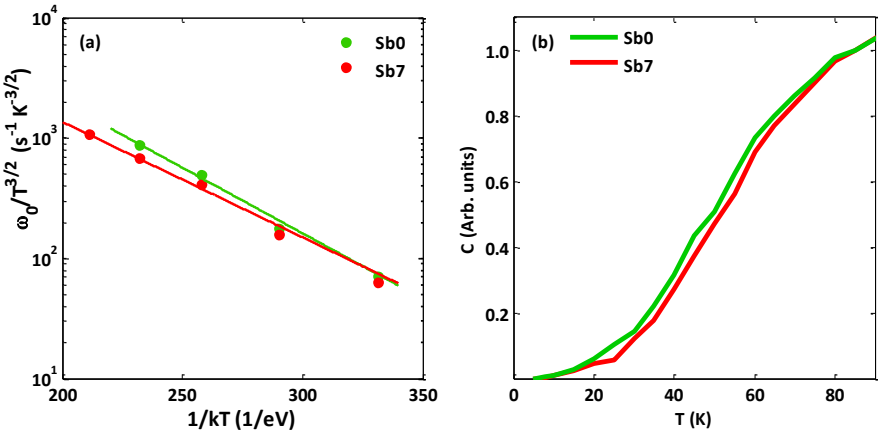

Figure 7: (a) Arrhenius diagram for m=3/2. (b) C-T spectra at frequency of 100 kHz and bias -0.3 V.

4 Conclusions

The thin-film CIGS solar cells investigated here were produced by a three stage co-evaporation process at reduced deposition temperature. An Sb layer with varying thickness (0, 7, 12 nm), which is expected to promote CIGS grain growth, was included prior to CIGS deposition. Enhanced EQE values on the long wavelength side for cells with Sb layer are probably related to the larger grain size in these cells, as demonstrated by SEM. PP-TOFMS depth profiling measurements revealed a very limited Sb diffusion in the CIGS absorber layer, however, a small Sb concentration was also observed in the surface region. Admittance measurements could not reveal a direct effect from Sb addition on the defect structure. Both in cells with and without Sb layer, a shallow acceptor level with activation energy estimated around 25±5 meV was found and assigned to the dominant acceptor in CIGS absorber, probably the V_{Cu} intrinsic defect.

Acknowledgments

The authors acknowledge the special university fund of UGent (BOF-01N01611) for financial support and O. Janssens (Ghent University) for support in the SEM experiments.

References

[1] Jackson P, Hariskos D, Wuerz R, Kiowski O, Bauer A, Friedlmeier T M and Powalla M 2014 Properties of Cu(In,Ga)Se_2 solar cells with new record efficiencies up to 21.7% *Phys. Status Solidi RRL* 1-4

[2] Chirila A, Reinhard P, Pianezzi F, Bloesch P, Uhl A R, Fella C, Kranz L, Keller D, Gretener C, Hagendorfer H, Jaeger D, Erni R, Nishiwaki S, Buecheler S and Tiwari A N 2013 Potassium-induced surface modification of Cu(In,Ga)Se_2 thin films for high-effciency solar cells *Nature Materials* **12** 1107-11

[3] Yuan M, Mitzi D B, Liu W, Kellock A J, Chey S J and Deline V R 2009 Optimization of CIGS-based PV device through antimony doping *Chem. Mater.* **22** 285-7

[4] Yuan M, Mitzi D B, Gunawan O, Kellock A J, Chey S J and Delin V R 2010 Antimony assisted low temperature processing of $CuIn_{1-x}Ga_xSe_{2-y}S_y$ solar cells *Thin Solid Films* **519** 852-6

[5] Nakada T, Honishi Y, Yatsushiro Y and Nakakoba H 2011 Impacts on Sb and Bi incorporations on CIGS thin films and solar cells *Photovoltaic Specialists Conf. (Seattle)* 3527-31

[6] Akaki Y, Komaki H, Yokoyama H, Yoshino K, Maeda K and Ikari T 2003 Structural and optical characterization of Sb-doped $CuInS_2$ thin films grown by vacuum evaporation method *Journal of Physics and Chemistry of Solids* **64** 1863-7

[7] Tseng B, Chang G, and Gu G 1996 Surfactant modified growth of $CuInSe_2$ thin films *Applied Surface Science* **92** 227-31

[8] Zhang S, Wu L, Yue R, Yan Z, Zhan H and Xiang Y 2013 Effects of Sb-doping on the grain growth of Cu(In, Ga)Se_2 thin films fabricated by means of single-target sputtering *Thin Solid Films* **527** 137-40

[9] Ben Rabeh M, Chaglabou N and Kanzari M 2009 Structural, optical and electrical properties of annealed Sb-doped $CuInS_2$ thin films grown by thermal evaporation method *Chalcogenide Lett* **6** 83-9

[10] Ben Rabeh M, Chaglabou N and Kanzari M 2010 Effect of antimony incorporation on structural properties of $CuInS_2$ crystals *Nucl. Instr. Meth. Phys. Res. B* **268** 273-6

[11] Komaki H, Yoshino K, Akaki Y, Yoneta M and Ikari T 2003 Characterization of Sb-doped $CuInS_2$ crystals *Phys. Stat. Sol. C* **0** 759-62

[12] Van Puyvelde L, Lauwaert J, Pianezzi F, Nishiwaki S, Smet P F, Poelman D, Tiwari A N and Vrielinck H

2014 Influence of an Sb doping layer in CIGS thin-film solar cells: a photoluminescence study *J. Phys. D: Appl. Phys.* **47** 045102

[13] Sakurai T, Ishida N, Ishizuka S, Matsubara K, Sakurai K, Yamada A, Paul G K, Akimoto K and Niki S 2007 Investigation of relation between Ga concentration and defect levels of Al/Cu(In,Ga)Se_2 Schottky junctions using admittance spectroscopy *Thin Solid Films* **515** 6208-11

[14] Cao Q, Gunawan O, Copel M, Reuter K B, Chey S J, Deline V R and Mitzi D B 2001 Defects in Cu(In,Ga)Se_2 chalcopyrite semiconductors: a comparative study of material properties, defect states and photovoltaic performance *Adv. Energy Mater.* **1** 845-53

[15] Eisenbarth T, Unold T, Caballero R, Kaufmann C A and Schock H W 2010 Interpretation of admittance, capacitance-voltage, and current-voltage signatures in Cu(In,Ga)Se_2 thin film solar cells *J. Appl. Phys.***107** 034509

[16] Zhang S B, Wei S and Zunger A 1998 Defect physics of the $CuInSe_2$ chalcopyrite semiconductor *Phys. Rev. B* **57** 9642-55

[17] Tempez A, Legendre S and Chapon P 2014 Depth profile analysis by plasma profiling time of flight mass spectrometry *Nucl. Instr. Meth. B* **332** 351-4

[18] Aninat R, Zoppi G, Tempez A, Chapon P, Beattie N S, Miles R and Forbes I 2013 Crystallographic Properties and Elemental Migration in two-stage prepared Cu($In_{1-x}Al_x$)Se_2 thin films for photovoltaic applications *Journal of Alloys and Compounds* **566** 180-6

[19] Kartopu G, Tempez A, Clayton A J, Barrioz V, Irvine S J C, Olivero C, Chapon P, Legendre S and Cooper J 2014 Chemical analysis of $Cd_{1-x}Zn_xS$/CdTe solar cells by plasma profiling TOFMS *Materials Research innovations* **18** 82-5

[20] Lauwaert J, Khelifi S, Decock K, Burgelman M and Vrielinck H 2011 Signature of a back contact barrier in DLTS spectra *J. Appl. Phys.* **109** 063721

[21] Lauwaert J, Callens L, Kheliffi S, Decock K, Chirila A, Pianezzi F, Buecheler S, Tiwari A N and Vrielinck H 2012 About RC-like contacts in deep level transient spectroscopy and Cu(In,Ga)Se_2 solar cells *Prog. Photovolt: Res. Appl.* **5** 588-94

[22] Herberholz R, Igalson M and Schock H W 1998 Distinction between bulk and interface states in

$CuInSe_2$/CdS/Zn0 by space charge spectroscopy *J. Appl. Phys.* **83** 318-25

[23] Igalson M and Zabierowski P 2003 Electron traps in Cu(In,Ga)Se_2 absorbers of thin film solar cells studied by junction capacitance techniques *Optoelectronics review.* **11** 261-7

[24] Heath J T, Cohen J D and Shafarman W N 2004 Bulk and metastable defects in $CuIn_{1-x}Ga_xSe_2$ thin films using drive-level capacitance profiling *J. Appl. Phys.* **95** 1000-10

[25] Reisloehner U, Metzner H and Ronning C 2004 Hopping conduction observed in thermal admittance spectroscopy *Phys. Rev. Lett.* **104** 226403

[26] Lee J W, Cohen J D and Shafarman W N 2005 The determination of carrier mobilities in CIGS photovoltaic devices using high-frequency admittance measurements *Thin Solid Films* **480** 336-40

[27] Abou-Ras D, Kirchartz T and Rau U 2011 Advanced Characterization Techniques for Thin Film Solar Cells (Weinheim, Germany, Wiley)

[28] Siebetritt S and Rau U 2006 Wide-Gap Chalcopyrites ed Hull R, Osgood R M et al (Berlin- Heidelberg, Springer)

[29] Li J V, Li X, Albin S S and Levi D H 2010 A method to measure resistivity, mobility, and absorber thickness in thin-film solar cells with application to CdTe devices *Sol. Energy Mater. Sol. Cells* **94** 2073-7

[30] Decock K, Khelifi S, Buecheler S, Pianezzi F, Tiwari A N and Burgelman M 2011 Defect distributions in thin film solar cells deduced from admittance measurements under different bias voltages *J. Appl. Phys.* **110** 063722

[31] Kodigala, S R 2010 Thin films and nanostructures $Cu(In_{1-x}Ga_x)Se_2$ based thin film solar cells (Oxford, UK, Academic Press)